Design of a cytotoxic neuroblastoma-targeting agent using an enzyme acting on polysialic acid fused to a toxin

Lehti, Timo

2021-10

Lehti , T , Pajunen , M , Jokilammi , A , Korja , M J , Lilie , H , Vettenranta , K & Finne , J 2021 , ' Design of a cytotoxic neuroblastoma-targeting agent using an enzyme acting on polysialic acid fused to a toxin ' , Molecular Cancer Therapeutics , vol. 20 , no. 10 , pp. 1996-2007 . https://doi.org/10.1158/1535-7163.MCT-20-1031

http://hdl.handle.net/10138/346431
https://doi.org/10.1158/1535-7163.MCT-20-1031

unspecified
acceptedVersion

Design of a cytotoxic neuroblastoma-targeting agent using an enzyme acting on polysialic acid fused to a toxin

Timo A. Lehti*, Maria I. Pajunen, Anne Jokilammi, Miikka Korja, Hauke Lilie, Kim Vettenranta, Jukka Finne
*Corresponding author

Affiliations:
Timo A. Lehti. Molecular and Integrative Biosciences Research Programme, Faculty of Biological and Environmental Sciences, University of Helsinki, Finland.
Maria I. Pajunen. Molecular and Integrative Biosciences Research Programme, Faculty of Biological and Environmental Sciences, University of Helsinki, Finland.
Anne Jokilammi. Institute of Biomedicine, Cancer Laboratories and Medicity Research Laboratories, Faculty of Medicine, University of Turku, Finland.
Miikka Korja. Department of Neurosurgery, Helsinki University Hospital, University of Helsinki, Finland.
Hauke Lilie. Institute of Biochemistry and Biotechnology, Martin Luther University Halle-Wittenberg, Halle (Saale), Germany.
Kim Vettenranta. University of Helsinki and Hospital for Children and Adolescents, Helsinki University Central Hospital, Helsinki, Finland.
Jukka Finne. Molecular and Integrative Biosciences Research Programme, Faculty of Biological and Environmental Sciences, University of Helsinki, Finland.

Running title: Enzyme–toxin conjugate targeting polysialic acid

Corresponding author: Timo A. Lehti. Mailing address: Molecular and Integrative Biosciences Research Programme, P.O. Box 56, FI-00014 University of Helsinki; email address: timo.lehti@helsinki.fi.

Conflict of interest statement: The authors declare no potential conflicts of interest.

Abstract

Polysialic acid, an abundant cell surface component of the developing nervous system, which declines rapidly postnatally to virtual absence in the majority of adult tissues, is highly expressed in some malignant tumors including neuroblastoma. We found that the binding of a non-catalytic endosialidase to polysialic acid causes internalization of the complex from the surface of neuroblastoma kSK-N-SH cells, a subline of SK-N-SH, and leads to a complete re-localization of polysialic acid to the intracellular compartment. The binding and uptake of the endosialidase is polysialic acid-dependent as it is inhibited by free excess ligand or removal of polysialic acid by active endosialidase, and does not happen if catalytic endosialidase is used in place of inactive endosialidase. A fusion protein composed of the non-catalytic endosialidase and the cytotoxic portion of diphtheria toxin was prepared in order to investigate whether the cellular uptake observed could be used for the specific elimination of polysialic acid-containing cells. The conjugate toxin was found to be toxic to polysialic acid positive kSK-N-SH with an IC_{50} of 1.0 nM. Replacing the non-catalytic endosialidase with active endosialidase decreased the activity to the level of non-conjugated toxin. Normal non-malignant cells were selectively resistant to the toxin conjugate. The results demonstrate that non-catalytic endosialidase induces a quantitative removal and cellular uptake of polysialic acid from the cell surface which, by conjugation with diphtheria toxin fragment, can be exploited for the selective elimination of polysialic acid-containing tumor cells.

Introduction

Alterations in cell surface glycosylation are potential targets for diagnostic and therapeutic strategies in cancer (1, 2). Polysialic acid is a linear homopolymer of N-acetylneuraminic acid and exists at the cell surface mainly as a part of the neural cell adhesion molecule NCAM (3, 4). As a negatively charged molecule with a large hydration volume, it interferes with NCAM-mediated cell–cell interactions and NCAM signalling (5). Polysialic acid is strongly expressed during embryonic development and plays a critical role in nervous system development and maintenance but is also involved in the development of other organs (6). The expression of polysialic acid declines rapidly after birth and persists mainly behind the blood-brain barrier in brain areas associated with plasticity and neurogenesis (7). Polysialic acid is also found in a number of malignant tumors, including neuroblastoma (8). Its expression in cancer cells generally correlates with malignancy and facilitates cell detachment, metastasis, invasion and tumor growth (9-11), and protects cells from humoral and cellular defense systems (12, 13). Because of the high prevalence of polysialic acid expression in clinical samples and the frequent association of elevated expression with poor prognosis, polysialic acid is a useful biomarker for neuroblastoma and many other types of tumors (8).

Neuroblastoma represents one of the most unique pediatric solid tumors with a broad spectrum of clinical behavior patterns ranging from a poorly understood spontaneous regression to fatal progression. About half of the patients are diagnosed with a metastatic high-risk phenotype (14) and despite intensive treatment strategies, the survival rates are poor (50–60% long-term survival) (15, 16). Novel treatment approaches such as therapies directed towards oncofetal antigens could improve the cure rates (13). The use of polysialic acid as a receptor for tumor-targeted oncolysis has recently emerged as a promising approach (17, 18). The internalization of polysialic acid provides an opportunity to use this oncofetal cell surface component as an entry port for cytotoxic payloads acting on malignant cells.

The development of antibodies for therapeutic applications is time-consuming and costly, and traditionally dependent on animal immunization (19, 20). As an alternative to antibodies, affinity reagents from various scaffolds have been designed to overcome the limitations of antibodies (21). Here, we have taken advantage of a known molecular interaction, the binding of an enzyme to its substrate, with the aim of targeting neuroblastoma. A catalytically disabled form of the polysialic acid cleaving enzyme endosialidase shows an antibody-like affinity toward α2,8-linked polysialic acid present on mammalian cells (22). The endosialidase from bacteriophage PK1A2 has two amino acid substitutions (H417Y and N489D) at the active site that abolish the polysialic acid cleaving activity but still permit the binding specifically to the substrate (23). We show that the endosialidase is selectively internalized into neuroblastoma cells in a polysialic acid-

dependent manner and is redistributed from the cell surface to intracellular compartments. Following a genetic fusion of a catalytic subunit of diphtheria toxin to the non-catalytic endosialidase through a furin-cleavable linker, we found that the conjugate is selectively cytotoxic for neuroblastoma cells expressing polysialic acid.

Material and Methods

DNA constructs

Construction of plasmids for expression of recombinant proteins is described in the Supplementary Materials and Methods. The oligonucleotides used are specified in Supplementary Table S1. All constructs were verified with PCR and sequencing.

Purification of fusion proteins

Constructs were expressed in *Escherichia coli* M15 (pREP4) expression strain as N-terminal histidine-tagged fusion proteins and purified under native conditions using nickel-nitrilotriacetic acid resin (Qiagen or Sigma-Aldrich) as described before (22). Protein samples were analyzed for integrity by SDS-PAGE with a 15% polyacrylamide resolving gel and stained with Coomassie brilliant blue. Protein concentrations were determined using the Pierce BCA Protein Assay Kit (Thermo Fisher Scientific).

Cell lines

Human neuroblastoma cell lines SK-N-SH (RRID:CVCL_0531), SK-N-AS (RRID:CVCL_1700) and SH-SY5Y (RRID:CVCL_0019), and human foreskin fibroblast cell line BJ (RRID:CVCL_3653) were purchased and authenticated from ATCC. kSK-N-SH, a subline of SK-N-SH enriched for polysialic acid-positive cells, was previously established and authenticated in our laboratory (24, 25). All cell lines were routinely tested mycoplasma-free using the EZ-PCR Mycoplasma Test Kit (Biological Industries) and passed less than 20 times. Cells were cultured at 37°C in 5% CO_2 in DMEM containing 4.5 g/L glucose (Sigma-Aldrich), supplemented with 10% FBS (HyClone), and 1% penicillin/streptomycin (Gibco).

Isolation of bone marrow mononuclear cells

Bone marrow (BM) was collected from two healthy volunteer donors after informed consent, using a protocol approved by the ethics committee of Helsinki University Central Hospital (Finland) and in accordance with the Declaration of Helsinki. BM aspirates collected under local anesthesia from the posterior iliac crest into a heparin-treated syringe were further processed in order to isolate the mononuclear cell fraction based on their capacity to adhere to the plastic surfaces. BM mononuclear cells were isolated either by direct seeding of untreated whole BM aspirate or using the red blood cell (RBC) lysis treatment with ammonium chloride. For direct culturing, 0.1 ml BM aspirate was suspended in 10 ml of culture medium (DMEM, 10% FBS, 1% penicillin/streptomycin), and cultured at 37°C in 5% CO_2. RBC lysis was performed by mixing 0.1 ml BM aspirate with 1 ml RBC lysing solution (150 mmol/L NH_4Cl, 10 mmol/L $NaHCO_3$, 0.1 mmol/L EDTA, pH 7.4) and incubating for 10 min on ice. Subsequently, cells were centrifuged

for 10 minutes at 250 × *g*, suspended in 10 ml of culture medium, and seeded in a 25 cm^2 flask. After 5–6 days, when single colonies of adherent fibroblast-like cells were visible, non-adherent cells were washed with PBS, and the culture medium was changed. Thereafter, the culture medium was replaced every 3–4 days, and the plastic-adherent mononuclear cells were subcultured at 70–90% confluence. In line with a previous study (26), no differences in cellular morphology and growth pattern were observed between untreated and RBC lysis cultures after the expansion of plastic-adherent mononuclear cells. Untreated whole BM adherent cultures were freshly used, up to passage 5, in downstream assays.

Cell viability assay

The cells were seeded into 96-well plates (5×10^4/well for kSK-N-SH, 3×10^4/well for SK-N-AS and SH-SY5Y, 1.5×10^4/well for BJ and BM mononuclear cells, and 1×10^4/well for SK-N-SH) and incubated at 37 °C in 5% CO_2. The next day, the culture medium was substituted with a fresh medium containing different concentrations of toxin conjugates or control protein for the time periods indicated. For short-term exposures (2 to 6 h), the cells were washed once with culture medium after treatment time, and the incubation was continued in fresh medium to 24 h. At the end of the incubation period, cell viability was determined by the 3-(4,5-dimetrylthiazol-2-yl)-2,5-diphenyltetrazoliumbromide (MTT, Sigma-Aldrich)-based assay as described before (25). Cell viability was calculated in relation to control (non-treated) cells. Half-maximal inhibitory concentration (IC_{50}) was determined by global nonlinear regression with a variable slope (four-parameter) method using Prism 8 software (GraphPad Software, RRID:SCR_002798).

Serum stability assay

DT386F-endoNA2 (0.7 mg/mL) was incubated in 50% normal human serum (H4522, Sigma-Aldrich) or 25 mmol/L sodium phosphate, pH 7.4, 150 mmol/L NaCl at 37°C. After various time intervals, the samples were analyzed in the cell viability assay on kSK-N-SH cells as described above. IC_{50} values were normalized to the control sample without incubation at 37°C (100% activity).

Fluorescence microscopy

For analysis of endosialidase internalization, cells grown on glass coverslips were incubated with 10 µg/mL GFP-endoNA2 in culture medium at 37°C in 5% CO2. After various time intervals, the cells were washed with PBS and fixed with cold 4% paraformaldehyde in PBS for 25 min at room temperature. After washing three times with PBS, the coverslips were mounted in ProLong Mounting Medium with DAPI (Molecular Probes). Images were acquired using Olympus BX50F-3 with Retiga 6000 CCD camera and analyzed using Image-Pro Plus 7.0 software (RRID:SCR_007369). As a control, cells were incubated in the presence of free bacterial polysialic acid (1 mg/mL colominic acid, poly-2,8-N-acetylneuraminic acid sodium salt, Sigma-

Aldrich). As a further control, cells were pretreated with V5-endoNA (10 µg/mL) for 3 h at 37°C in 5% CO_2 in order to remove cell surface polysialic acid.

For the staining of cell surface polysialic acid, fixed cells were blocked with 1.5% normal horse serum (Vector Laboratories) in PBS for 1 h at room temperature and then stained with 10 µg/mL DsRed-endoNA2 or GFP-endoNA2 in PBS for 1 h at room temperature. Then, cells were processed for visualization in a fluorescence microscope as described below.

For low-temperature experiments, cells were washed with cold PBS and preincubated in cold culture medium for 30 min at 4°C prior to incubation with 10 µg/mL GFP-endoNA2 at 4°C. For depletion of ATP, cells were washed with PBS, preincubated with an ATP depletion solution [10 mmol/L sodium azide (Sigma-Aldrich) and 50 mmol/L 2-deoxy-D-glucose (Sigma-Aldrich) in culture medium] for 1 h at 37 °C in 5% CO_2 and then incubated with 10 µg/mL GFP-endoNA2 for 1 h. The mitochondrial ATP production was also perturbed by treatment of cells with 10 µmol/L CCCP. In parallel control experiment, the incubation was preceded by a 15-min incubation with 50 nmol/L MitoTracker Red CMXRos (Thermo Fisher Scientific). For the inhibition of endosomal acidification, cells were preincubated with 10 mmol/L NH_4Cl or 100 µmol/L chloroquine for 15 min in a 37°C in 5% CO_2 and further incubated with 10 µg/mL GFP-endoNA2 for 1 h. To assess the effect of NH_4Cl on the acidification, cells were stained with 1 µg/mL acridine orange (Sigma-Aldrich) for 15 min at 37°C in 5% CO_2, washed twice with PBS, mounted on PBS and immediately visualized under fluorescence microscope.

For EEA1 or V5 immunolabelling, cells were fixed with paraformaldehyde and permeabilized with 0.1% Triton X-100, 1.5% normal horse serum in PBS for 1 h at room temperature. Cells were then incubated with rabbit monoclonal anti-EEA1 (1:200; Cell Signaling, RRID:AB_2096811) overnight at 4°C or rabbit polyclonal anti-V5 (1:500; Millipore, RRID:AB_91591) for 2 h at room temperature. The secondary antibody Alexa-Fluor 555 goat anti-rabbit (Molecular Probes, RRID:AB_2535850) was used at 1:500 for 2 h. After washing three times with PBS, coverslips were mounted on slides.

For removing cell membrane-bound inactive endosialidase fusion proteins before fixation, polysialic acid competition treatment (1 mg/mL colominic acid in culture medium) was used as described before (25), except that the incubations were done at room temperature.

For detection of apoptosis, cells were stained using an Alexa-Fluor 488 annexin V and propidium iodide kit (Thermo Fisher Scientific) or 2 µmol/L CellEvent caspase-3/7 green detection reagent (Thermo Fisher

Scientific) in combination with 5 µmol/L Hoechst 33258 (Sigma-Aldrich) following the manufacturer's protocols. For quantification of apoptosis, non-fixed cells were examined under fluorescence microscope and marker stainings from at least 300 different cells were counted for each individual experiment.

For quantification of N- and S-type cell populations of kSK-N-SH, an image-based cell profiling was used. N-type cells are characterized by a small, rounded cell body with numerous neuritic processes and a low cytoplasm/nuclei ratio, whereas S-type cells are larger, flattened cells with abundant cytoplasm and larger nuclei. Nuclei were identified by DAPI staining and calculated using an automated image analysis pipeline implemented in CellProfiler 2.0.1 software (ref. 27, RRID:SCR_007358). The cell types were differentiated based on their nuclear size. Manual analysis of cellular morphology in phase-contrast images was used to confirm the profiling.

Flow cytometry

Polysialic acid detection by flow cytometry was performed as described previously (24). Briefly, cells were detached from the culture dish with 2.5 mg/mL trypsin-EDTA (Gibco) for 5 min at 37°C, followed by neutralization by adding culture medium. Cells were stained with 10 µg/mL GFP-endoNA2 in PBS for 1 h on ice, washed twice with PBS, and resuspended in 500 µl PBS for analysis on FACS LSR II flow cytometer (BD Biosciences) operated by FACSDiva 5.0.3 software (RRID:SCR_001456).

Statistical analysis

An unpaired two-tailed Student´s *t* test was used to determine significance. *P* values <0.05 were considered statistically significant.

Results

Antibody-mimetic endosialidase endoNA2 is effectively internalized into polysialic acid-expressing cells

We first examined if the non-catalytic endosialidase endoNA2 fused to GFP would be internalized into kSK-N-SH cells, a human neuroblastoma cell line that has been isolated from the SK-N-SH cell line by immunomagnetic bead separation (24). A vast majority (94–98%) of the kSK-N-SH cells express polysialic acid (Supplementary Fig. S1) as well as NCAM and have a neuroblastic (N-type) morphology (24, 25). The kSK-N-SH cell line also contains a minor polysialic acid-negative population of cells having a flat substrate-adherent (S-type) phenotype. Before the initiation of internalization (0 min), polysialic acid was visualized with DsRed-endoNA2 in a diffuse pattern along the cell surface of the N-type cells (**Fig. 1A**). Upon incubation with GFP-endoNA2 at 37°C for 15 min, decreased level of cell surface polysialic acid was observed and was coincided with a granular-like appearance of the label. After the next 15 min, GFP-endoNA2 was visible in the form of discrete clusters at the periphery of the cell nucleus, whereas all polysialic acid staining was removed from the cell surface. Over 24 h of incubation, the clustered fluorescence signal increased (**Fig. 1A**), which suggested accumulation of GFP-endoNA2 in perinuclear vesicular compartments. The S-type cells of kSK-N-SH were negative for polysialic acid and internalization of GFP-endoNA2 (**Fig. 1A**). No internalization was observed when kSK-N-SH cells were incubated with a fusion protein containing catalytically active endosialidase (**Fig. 1B**).

To test whether the internalization of the antibody-mimetic endosialidase fusion protein was mediated by cell surface-expressed polysialic acid, we pretreated kSK-N-SH cells with catalytically active endosialidase endoNA, an enzyme that removes polysialic acid from the cell surface (22, 25, 28). In the endosialidase-treated cells, the internalization of GFP-endoNA2 was completely abolished (**Fig. 1C**). Furthermore, addition of excess soluble polysialic acid inhibited the internalization into kSK-N-SH cells. Consistent with these results, neuroblastoma SK-N-AS (S-type) cells lacking polysialic acid (ref. 25; Supplementary Fig. S1) did not take up GFP-endoNA2 (**Fig. 1D**).

Next, kSK-N-SH cells were pre-incubated at 4°C to arrest endocytosis. Following incubation with GFP-endoNA2 for 1 h at 4°C, the fluorescence signal localized to the plasma membrane and no punctate staining pattern of uptake was evident, which suggested that an energy-driven process is responsible for the uptake of the endosialidase fusion protein (**Fig. 1E**). As a further test, kSK-N-SH cells were treated with sodium azide and 2-deoxy-D-glucose. The mixture, which impairs the production of cellular ATP, reduced the uptake of GFP-endoNA2 (**Fig. 1E**). A similar result was observed after depletion of cellular energy with the

protonophore carbonyl cyanide m-chlorophenyl hydrazone (CCCP) that collapses the mitochondrial membrane potential and uncouples oxidative phosphorylation. In parallel control experiment, staining with the mitochondrial membrane potential-sensitive dye MitoTracker Red CMXRos demonstrated that the CCCP treatment was efficient at depolarizing the mitochondria.

Taken together, the results suggest that the binding of non-catalytic endosialidase–fluorescent protein conjugate to cell surface polysialic acid causes its active internalization from the cell surface and leads to a rapid and complete redistribution of polysialic acid to the intracellular compartments, at least to a significant portion via an endocytic energy-driven mechanism.

Trafficking of GFP-endoNA2 involves endosomal acidification

To determine the intracellular distribution of GFP-endoNA2, the localization of internalized GFP-endoNA2 was compared with the early endosome marker EEA1. As shown in **Fig. 2A**, many of the GFP-fluorescent puncta overlapped with the fluorescence of EEA1, which suggested the localization of GFP-endoNA2 in early endosomes.

Endosome maturation involves a progressive acidification of the vacuole lumen (29). To examine whether acidification of the early endosomes is necessary for the cellular uptake of GFP-endoNA2, we used lysosomotropic weak bases that penetrate acidic compartments of the cell and elevate their lumenal pH. Upon treating the cells with the lysosomotropic agent ammonium chloride (NH_4Cl) the internalization of GFP-endoNA2 was impaired (**Fig. 2B**). The alkalinization of intraorganellar pH by NH_4Cl was confirmed by staining with acridine orange, an acidotropic dye that concentrates in acidic vesicles and is used as an indicator of acidification. Untreated control cells stained with acridine orange exhibited typical bright orange fluorescence of acid compartments, whereas no such fluorescence was observed in cells treated with NH_4Cl (**Fig. 2B**). Inhibition of endosomal acidification by the inhibitor chloroquine also reduced the entry of GFP-endoNA2 into target cells, which further supports the potential involvement of a low pH-dependent step in the endocytic pathway of GFP-endoNA2.

Construction of endosialidase–toxin conjugates and comparison of their cytotoxicity

The internalization properties of GFP-endoNA2 suggest that the non-catalytic endosialidase could act as a targeting moiety and drug carrier to deliver membrane impermeable drugs into malignant polysialic acid-expressing cells. To develop a polysialic acid-targeted toxin conjugate, we replaced the GFP domain with

truncated forms of two alternative bacterial toxins, diphtheria toxin DT386 and *Pseudomonas* exotoxin A PE38, which contain the catalytic and translocation domains of the toxins (30). Upon cellular internalization, inefficient trafficking of toxic substances from endosomes into the cytosol may limit the efficacy of the targeted toxin. Therefore, we also designed conjugates that have a cleavable linker between the toxin domain and the spacer to enhance the intracellular release of the catalytically active toxin fragment from the targeting domain. In these conjugates, either the furin cleavage motif RVRR (31) or the caspase-3/7 cleavage motif DEVD (32, 33) were used as the linker. For PE38, the native endoplasmic reticulum retention sequence REDLK at the C-terminus was also substituted with the canonical KDEL sequence (34). A schematic representation of the constructs is shown in **Fig. 3A**. The purified conjugates showed their predicted molecular weights in denaturing SDS-PAGE separations (Supplementary Fig. S2).

The DT386- and PE38-based conjugates were tested for their tumor antigen-specific killing activity on kSK-N-SH cells. We found that the DT386 conjugates induced dose-dependent cytotoxicity, with the half-maximal inhibitory concentrations (IC_{50}) ranging from 1.0 to 36 nM (**Fig. 3B**). No cytotoxicity was observed in the presence of control GFP-endoNA2. The incorporation of a cleavable linker between the DT386 domain and the spacer improved cytotoxicity approximately 18- to 35-fold compared to the toxin conjugate without the linker. The DT386F-endoNA2 containing a furin-cleavable linker showed the highest cytotoxicity (IC_{50} = 1.0 nM). In contrast, regardless of the presence of the furin cleavage site or the endoplasmic reticulum retention sequence KDEL, PE38-based conjugates were 3- to 2-log less cytotoxic than DT386F-endoNA2 (**Fig. 3C**).

The receptor and catalytic domains of PE are arranged in an orientation opposite to that of DT, and proper orientation in recombinant PE fusion proteins may be required for efficient delivery of the toxin moiety into the cytosol (35). A short C-terminal domain of endosialidases functions as an intramolecular chaperone and is proteolytically released at a highly conserved serine residue during protein maturation, however, the cleavage can be prevented by a single point mutation (36). Introducing the corresponding amino acid substitution S706A to endoNA2 had no significant effect on binding and internalization into the kSK-N-SH cells (Supplementary Fig. S3A,B). Next, the mutant endosialidase endoNA2-S706A with V5-epitope was linked by the furin site to the N-terminus of PE38-KDEL (see **Fig. 3A**). Notably, the cytotoxicity of the resulting fusion protein V5-endoNA2-S706A-FPE38K was 11-fold higher than that of PE38KF-endoNA2 (**Fig. 3C**), which suggests a positional effect of the receptor-binding domain on toxin activity. However, the observed cytotoxicity was still 70-fold less than with DT386F-endoNA2.

An important factor for the clinical efficacy of any targeted toxin therapeutic is the time required for target cells to internalize and deliver the toxin to the cytosol. To determine if short-term exposure to DT386F-endoNA2 would be sufficient for cytotoxicity, kSK-N-SH cells were incubated with DT386F-endoNA2 for various intervals up to 6 h after which the conjugate was removed and incubation continued to 24 h, allowing time for the internalized conjugate to block protein synthesis and induce cell death. For comparison, cells were incubated continuously for 24 or 48 h with the conjugate. Already after 2 h exposure, the kSK-N-SH cells showed a strong dose-dependent loss of viability (IC_{50} = 7.9 nM; **Fig. 3D**). Increasing the exposure time from 2 h to 6 h decreased the IC_{50} 4-fold whereas extending the exposure time to 24 or 48 h resulted in 8- and 11-fold decline, respectively. Altogether, cytotoxicity observed at low nanomolar concentrations reflects that short exposure to DT386F-endoNA2 is sufficient to kill most of the polysialic acid-positive kSK-N-SH cells. The serum stability of DT386F-endoNA2 was subsequently determined by incubating the conjugate in human serum at 37°C for different time periods and then measuring cytotoxic activity. The conjugate retained more than 75% of the initial activity after 72 hours of incubation (Supplementary Fig. S4).

We next questioned whether the pronounced decrease in cell viability upon treatment with DT386F-endoNA2 was a result of apoptotic cell death. Annexin V and propidium iodide stainings were significantly increased by the 24-h toxin conjugate treatment in a concentration-dependent manner compared to the control (**Fig. 3E** and Supplementary Fig. S5A). We confirmed similar induction of apoptosis using a fluorogenic caspase-3/7 substrate to examine activation of apoptotic caspase-3 and caspase-7 (**Fig. 3F** and Supplementary Fig. S5B).

Cell binding and uptake of endosialidase–diphtheria toxin conjugate

To verify that DT386F-endoNA2 effectively targets polysialic acid-expressing cells, a V5-epitope tag for immunofluorescence detection was introduced at the N-terminus of the protein. The cytotoxicity of the V5-epitope-tagged conjugate against kSK-N-SH cells (IC_{50} = 1.6 nM; **Fig. 4A**) was comparable with that of DT386F-endoNA2. V5-DT386F-endoNA2 bound to the neuroblastic N-type cells of kSK-N-SH (**Fig. 4B**). The binding pattern was similar to that observed for V5-endoNA2, a control endosialidase without the DT386 domain, which suggests that the binding properties of the endosialidase domain were not altered as a result of the toxin domain fusion.

Next, we investigated the internalization of V5-DT386F-endoNA2 in live kSK-N-SH cells by immunofluorescence microscopy. After 2 h at 37°C, the toxin conjugate was internalized by the N-type cells similarly to the control endosialidase (**Fig. 4C**). In cells incubated at 4°C, bound V5-DT386F-endoNA2 remained confined to the cell surface, as indicated by its pericellular distribution and sensitivity to soluble polysialic acid. When the incubation time was increased to 24 h, a marked difference between the toxin conjugate and control protein was seen at 37°C. The treatment with V5-DT386F-endoNA2 caused shrinkage and rounding of the N-type cells, and there were fewer cells remaining (**Fig. 4C**), consistent with the cytotoxicity results (**Fig. 4A**). Also a visible reduction of the staining of the conjugate was observed within the cells, possibly because of protein degradation in the dying cells.

To further address the effect of the conjugate on the N- and S-type cell populations of kSK-N-SH, we lowered the conjugate concentration and extended the treatment time to 72 h. As a result, DT386F-endoNA2 completely eliminated the N-type cells while S-type cells not expressing polysialic were selectively resistant to the conjugate and outgrew the N-type cells after prolonged exposure to the conjugate (**Fig. 4D**). In parallel control experiments, DsRed-endoNA2 was internalized into the cells and consequently polysialic acid disappeared from the cell surface, while the proportion of N- and S-type cell subtypes remained unchanged. Collectively, these results indicate that DT386F-endoNA2 recognized polysialic acid and had the capacity to mediate killing of the target cells.

Cytotoxic activity and specificity of the DT386F-endoNA2 conjugate on various cell lines

To explore the cytotoxic capacity of DT386F-endoNA2 on cells with different polysialic acid expression levels, a panel of human neuroblastoma and primary cells were chosen. In contrast to the kSK-N-SH cells with high expression of polysialic acid, the neuroblastoma cell line SH-SY5Y expresses intermediate and SK-N-SH low levels of polysialic acid (ref. 25; Supplementary Fig. S1). Polysialic acid is undetectable in neuroblastoma SK-N-AS cells and BJ fibroblasts (ref. 25; Supplementary Fig. S1). In addition, we evaluated the toxicity of DT386F-endoNA2 treatment on two freshly isolated human bone marrow mononuclear cell populations. Analysis by flow cytometry revealed that 1% or less of these cells were cell surface-positive for polysialic acid (Supplementary Fig. S1), consistent with data from a previous report (37).

In accordance with polysialic acid expression, DT386F-endoNA2 effectively killed SH-SY5Y and SK-N-SH cells (IC_{50} = 8.0 nM and 12.6 nM, respectively; **Fig. 5A**) but not BJ fibroblasts or primary bone marrow mononuclear cells (IC_{50} >9000 nM; **Fig. 5B**). Although SK-N-AS neuroblastoma cells are negative for polysialic acid on the cell surface, we found that DT386F-endoNA2 led to an apparent decrease in the

viability of these cells (IC_{50} = 67 nM). In contrast, no cytotoxicity was observed for the toxin-free conjugate V5-endoNA2.

The cytotoxic effect of DT386F-endoNA2 on SK-N-AS cells suggests that either a proportion of SK-N-AS cells has very low, undetectable polysialic acid levels sufficient to target the conjugate into the cells or the conjugate has a polysialic acid-independent activity mediated by the diphtheria toxin domain itself (38). To prevent polysialic acid-specific internalization, we replaced the non-catalytic endosialidase endoNA2 in the conjugate with the active form endoNA. We also expressed the toxin domain DT386 without an endosialidase domain. kSK-N-SH cells showed sensitivity to both DT386F-endoNA and DT386 (**Fig. 6A**). Compared to the polysialic acid-targeted DT386F-endoNA2, DT386F-endoNA was 41-fold and DT386 24-fold less toxic to the cells after 24-hours exposure. Shortening exposure times resulted in relatively minor effects on the IC_{50}s of DT386F-endoNA or DT386 (**Fig. 6B**).

These results indicate that the nontargeted truncated DT without a receptor-binding domain has an intrinsic capability to decrease the viability of the kSK-N-SH cells, albeit the cytotoxicity is greatly enhanced by targeting cell surface polysialic acid with non-catalytic endosialidase. We therefore directed our attention toward the DT386 domain and tested two more neuroblastoma cell lines as well as two primary cell populations. Despite the different expression status of polysialic acid, DT386 had similar cytotoxicity on both neuroblastoma cell lines (**Fig. 6C**). Notably, in SK-N-AS cells, DT386 elicited the same cytotoxic effect as the endosialidase conjugated toxin. In line with a previous study (38), the tested primary cells were not sensitive to DT386 (**Fig. 6D**). Combined, these findings demonstrate that the endosialidase–diphtheria toxin conjugate DT386F-endoNA2 has a selectivity profile that confers high potency for killing polysialic acid-expressing cancer cells while sparing normal healthy cells *in vitro*.

Discussion

We show here that non-catalytic endosialidase endoNA2, a unique type of antibody substitute, selectively internalizes into neuroblastoma cells and that toxin-endoNA2 conjugates represent a potent strategy for the elimination of polysialic acid-containing cells. Like other bacteriophage-derived endosialidases, the tumor-targeting moiety endoNA2 demonstrates high substrate specificity, binding with high affinity to α2,8-linked polysialic acid but not to other cell surface sialic acids (28). The low nanomolar binding affinity (the dissociation constant K_D of 19 nM) of endoNA2 is comparable with carbohydrate-binding antibodies (22). In the present study, we found that endoNA2 is readily internalized by endocytosis into cells expressing polysialic acid. Comparison of the endoNA2 internalization events to those of *E. coli* PK1A2 bacteriophage harboring non-catalytic endosialidase as a tailspike protein (25) shows that endoNA2 leads to a faster induction of internalization, removing the receptors from the cell surface in 30 min. The ability of endoNA2 to effectively route a protein cargo (GFP) to the endosomal system led us to test its ability to deliver toxic components into the target cell. We used two A–B toxins of bacterial origin, diphtheria toxin and *Pseudomonas* exotoxin A, that have been widely used in the development of immunotoxins for targeted cancer therapies. To date, three such immunotoxins have gained FDA approval for clinical use (39).

To promote intracellular processing of the chimeric toxins and thereby endosomal escape of the toxin domain, a proteolytically cleavable spacer was incorporated between the toxin domain and endoNA2. We found that the targeted toxin DT386F-endoNA2 composed of truncated diphtheria toxin coupled with a furin site to endoNA2 was superior and selective in its activity against polysialic-acid positive neuroblastoma cells at low nM concentrations while maintaining reasonable serum stability. With PE38, an opposite orientation of the toxin and receptor-binding domain was found to be crucial for cytotoxicity, presumably due to the dependence of a free C-terminus with an ER localization signal for successful intracellular trafficking of the toxin to the cytosol (40).

The tumor-cell specificity of DT386F-endoNA2 was based on two mechanisms of recognition: polysialic acid-binding via the non-catalytic endosialidase portion (22) and binding to the surface of cancer cells via the “receptorless" toxin (38). For the latter, the underlying mechanisms are not known but have been suggested to include pH-dependent membrane insertion of the translocation domain that is induced by extracellular acidification near cancer cell surfaces (41), or interaction of the translocation domain with caveolin-1 (42). Most importantly, DT386F-endoNA2 did not show toxicity toward normal polysialic acid-negative cells while the toxin conjugate exhibited a drastic induction of apoptosis in neuroblastoma cells.

However, it should be pointed out that most neuroblastomas consist of two phenotypically divergent tumor cell types, adrenergic (ADRN) neuroblastoma cells and mesenchymal (MES) tumor cells corresponding to the neuroblastic N-type cells and substrate-adherent S-type cells, respectively (43, 44). Remarkably, both cell types have the flexibility to spontaneously interconvert between the different cellular states, and this plasticity may be crucial for the development of resistance to standard therapies (44). Although DT386F-endoNA2 is primarily targeted to polysialic acid-positive cells that are associated with increased invasive and metastatic potential and advanced stages of disease (8), the conjugate was also found to exert a moderate negative effect on S-type cell proliferation due to its dual recognition capacity. Targeting both neuroblastoma cell types, in combination with current treatment modalities, is a promising strategy to increase treatment precision for patients with high-risk neuroblastoma (43). Further studies will be needed to evaluate the effects of DT386F-endoNA2 on tumor growth in preclinical models of neuroblastoma.

As a major regulator of cell interactions via the formation of a repulsive field, polysialylation on cancer cells provides a selective advantage for cell motility, invasion, metastasis and survival (5, 9, 45, 46). Similar to neuroinvasive bacteria expressing polysialic acid as a capsular structure (47), polysialic acid decoration of the cell surface likely protects cancer cells from immune defense mechanisms by physically restricting access to cell membrane structures (8). Notably, endoNA2 not only targets the toxin inside the cell but also voids the cell surface of polysialic acid. The ability of endoNA2 to quantitatively sweep the cell surface polysialic acid into the cell's interior could interfere with the malignant behavior of the target cells additionally as a consequence of this mechanism. Given the heterogeneity within tumor tissue, it is likely that the uneven distribution of targeted toxin could result in partial removal of polysialic acid in many of the target cells, in contrast to the complete sweep seen *in vitro*. Tumor-associated antigens exposed by removal of the shielding polysialic acid layer could potentially make these cells more vulnerable to immune attack (48).

Recently, an oncolytic adenovirus was armed with a polysialic acid-degrading endosialidase from the bacteriophage K1F and showed to have a promising therapeutic efficacy in treating neuroblastoma in a mouse model (17). Another study utilizing polysialic acid-directed antibodies for the introduction of small drug molecules into target cells demonstrated polysialic acid-specific cell killing of SH-SY5Y neuroblastoma cells, with an IC_{50} value of 17 nM (18). Here we sought to explore a novel approach based on the non-catalytic enzyme that has retained its substrate-binding specificity as a vehicle of selective cellular uptake. Two naturally occurred amino acid substitutions have converted the endosialidase catalytically inactive (23), still allowing high binding affinity to mammalian polysialic acid (22). Considering the rapid

accumulation of publicly available three-dimensional structures of enzymes, and particularly known catalytic sites (49), enzyme–substrate interactions could offer a so far essentially unexplored approach for targeting drugs, proteins and nucleic acids into cells. Due to the simplicity and rapidity of site-directed mutagenesis techniques and efficiency of protein expression systems, this protein engineering strategy provides an advantage compared to conventional antibody generation methods.

In conclusion, through the use of a polysialic-acid targeting non-catalytic enzyme, we have developed the first-in-class targeted toxin that efficiently inhibits the cell viability of neuroblastoma cell lines. While our study focuses on neuroblastoma, several other polysialic acid-expressing malignant cell types could potentially also be targeted. The conjugate may also find use under experimental setups for the selective targeting of polysialic acid-containing normal cells. Our findings pose targeting of polysialic acid as a strategy for improving treatment options for neuroblastoma and other cancers that overexpress this glycan. Exploring the enzyme-promoted recognition of cancer antigens may provide a promising alternative to antibodies and an avenue to generate targeted therapies.

Acknowledgements

This study was supported by the Academy of Finland (Grant 138365), the Magnus Ehrnrooth Foundation, Finska Läkaresällskapet, and the University of Helsinki through the Cell membrane recognition and dynamics research community (Membrec). The authors thank Pirjo Rahkola and Auli Nick for technical assistance.

References

1. Pinho SS, Reis CA. Glycosylation in cancer: Mechanisms and clinical implications. Nat Rev Cancer 2015;**15**:540–55.

2. Costa AF, Campos D, Reis CA, Gomes C. Targeting glycosylation: A new road for cancer drug discovery. Trends Cancer 2020;**6**:757–66.

3. Finne J. Occurrence of unique polysialosyl carbohydrate units in glycoproteins of developing brain. J Biol Chem 1982;**257**:11966–70.

4. Rutishauser U. Polysialic acid in the plasticity of the developing and adult vertebrate nervous system. Nat Rev Neurosci 2008;**9**:26–35.

5. Colley KJ, Kitajima K, Sato C. Polysialic acid: Biosynthesis, novel functions and applications. Crit Rev Biochem Mol Biol 2014;**49**:498–532.

6. Galuska CE, Lütteke T, Galuska SP. Is polysialylated NCAM not only a regulator during brain development but also during the formation of other organs? Biology (Basel) 2017;**6**:10.3390/biology6020027.

7. Schnaar RL, Gerardy-Schahn R, Hildebrandt H. Sialic acids in the brain: Gangliosides and polysialic acid in nervous system development, stability, disease, and regeneration. Physiol Rev 2014;**94**:461–518.

8. Falconer RA, Errington RJ, Shnyder SD, Smith PJ, Patterson LH. Polysialyltransferase: A new target in metastatic cancer. Curr Cancer Drug Targets 2012;**12**:925–39.

9. Elkashef SM, Allison SJ, Sadiq M, Basheer HA, Ribeiro Morais G, Loadman PM, et al. Polysialic acid sustains cancer cell survival and migratory capacity in a hypoxic environment. Sci Rep 2016;**6**:33026.

10. Eggers K, Werneburg S, Schertzinger A, Abeln M, Schiff M, Scharenberg MA, et al. Polysialic acid controls NCAM signals at cell-cell contacts to regulate focal adhesion independent from FGF receptor activity. J Cell Sci 2011;**124**:3279–91.

11. Seidenfaden R, Krauter A, Schertzinger F, Gerardy-Schahn R, Hildebrandt H. Polysialic acid directs tumor cell growth by controlling heterophilic neural cell adhesion molecule interactions. Mol Cell Biol 2003;**23**:5908–18.

12. Fukuda M. Possible roles of tumor-associated carbohydrate antigens. Cancer Res 1996;**56**:2237–44.

13. Cheung NK, Dyer MA. Neuroblastoma: Developmental biology, cancer genomics and immunotherapy. Nat Rev Cancer 2013;**13**:397–411.

14. Park JR, Bagatell R, Cohn SL, Pearson AD, Villablanca JG, Berthold F, et al. Revisions to the international neuroblastoma response criteria: A consensus statement from the national cancer institute clinical trials planning meeting. J Clin Oncol 2017;**35**:2580–7.

15. Matthay KK, Maris JM, Schleiermacher G, Nakagawara A, Mackall CL, Diller L, et al. Neuroblastoma. Nat Rev Dis Primers 2016;**2**:16078.

16. Ladenstein R, Pötschger U, Valteau-Couanet D, Luksch R, Castel V, Yaniv I, et al. Interleukin 2 with anti-GD2 antibody ch14.18/CHO (dinutuximab beta) in patients with high-risk neuroblastoma (HR-NBL1/SIOPEN): A multicentre, randomised, phase 3 trial. Lancet Oncol 2018;**19**:1617–29.

17. Martin NT, Wrede C, Niemann J, Brooks J, Schwarzer D, Kühnel F, et al. Targeting polysialic acid-abundant cancers using oncolytic adenoviruses with fibers fused to active bacteriophage borne endosialidase. Biomaterials 2018;**158**:86–94.

18. Cox EC, Thornlow DN, Jones MA, Fuller JL, Merritt JH, Paszek MJ, et al. Antibody-mediated endocytosis of polysialic acid enables intracellular delivery and cytotoxicity of a glycan-directed antibody-drug conjugate. Cancer Res 2019;**79**:1810–21.

19. Jain T, Sun T, Durand S, Hall A, Houston NR, Nett JH, et al. Biophysical properties of the clinical-stage antibody landscape. Proc Natl Acad Sci U S A 2017;**114**:944–9.

20. Rabia LA, Desai AA, Jhajj HS, Tessier PM. Understanding and overcoming trade-offs between antibody affinity, specificity, stability and solubility. Biochem Eng J 2018;**137**:365–74.

21. Simeon R, Chen Z. In vitro-engineered non-antibody protein therapeutics. Protein Cell 2018;**9**:3–14.

22. Jokilammi A, Ollikka P, Korja M, Jakobsson E, Loimaranta V, Haataja S, et al. Construction of antibody mimics from a noncatalytic enzyme-detection of polysialic acid. J Immunol Methods 2004;**295**:149–60.

23. Jakobsson E, Jokilammi A, Aalto J, Ollikka P, Lehtonen JV, Hirvonen H, et al. Identification of amino acid residues at the active site of endosialidase that dissociate the polysialic acid binding and cleaving activities in *escherichia coli* K1 bacteriophages. Biochem J 2007;**405**:465–72.

24. Skog MS, Nystedt J, Korhonen M, Anderson H, Lehti TA, Pajunen MI, et al. Expression of neural cell adhesion molecule and polysialic acid in human bone marrow-derived mesenchymal stromal cells. Stem Cell Res Ther 2016;**7**:113.

25. Lehti TA, Pajunen MI, Skog MS, Finne J. Internalization of a polysialic acid-binding *escherichia coli* bacteriophage into eukaryotic neuroblastoma cells. Nat Commun 2017;**8**:1915.

26. Horn P, Bork S, Diehlmann A, Walenda T, Eckstein V, Ho AD, et al. Isolation of human mesenchymal stromal cells is more efficient by red blood cell lysis. Cytotherapy 2008;**10**:676–85.

27. Kamentsky L, Jones TR, Fraser A, Bray M, Logan D, Madden K, et al. Improved structure, function, and compatibility for CellProfiler: modular high-throughput image analysis software. Bioinformatics 2011;**27**:1179–80.

28. Jakobsson E, Schwarzer D, Jokilammi A, Finne J. Endosialidases: Versatile tools for the study of polysialic acid. Top Curr Chem 2015;**367**:29–74.

29. Huotari J, Helenius A. Endosome maturation. EMBO J 2011;**30**:3481–500.

30. Antignani A, Fitzgerald D. Immunotoxins: The role of the toxin. Toxins (Basel) 2013;**5**:1486–502.

31. Thomas G. Furin at the cutting edge: From protein traffic to embryogenesis and disease. Nat Rev Mol Cell Biol 2002;**3**:753–66.

32. McStay GP, Salvesen GS, Green DR. Overlapping cleavage motif selectivity of caspases: Implications for analysis of apoptotic pathways. Cell Death Differ 2008;**15**:322–31.

33. Kwon MK, Nam JO, Park RW, Lee BH, Park JY, Byun YR, et al. Antitumor effect of a transducible fusogenic peptide releasing multiple proapoptotic peptides by caspase-3. Mol Cancer Ther 2008;**7**:1514–22.

34. Kreitman RJ, Pastan I. Importance of the glutamate residue of KDEL in increasing the cytotoxicity of *pseudomonas* exotoxin derivatives and for increased binding to the KDEL receptor. Biochem J 1995;**307 (Pt 1)**:29–37.

35. Chaudhary VK, Jinno Y, FitzGerald D, Pastan I. Pseudomonas exotoxin contains a specific sequence at the carboxyl terminus that is required for cytotoxicity. Proc Natl Acad Sci U S A 1990;**87**:308–12.

36. Mühlenhoff M, Stummeyer K, Grove M, Sauerborn M, Gerardy-Schahn R. Proteolytic processing and oligomerization of bacteriophage-derived endosialidases. J Biol Chem 2003;**278**:12634–44.

37. Korja M, Jokilammi A, Salmi TT, Kalimo H, Pelliniemi TT, Isola J, et al. Absence of polysialylated NCAM is an unfavorable prognostic phenotype for advanced stage neuroblastoma. BMC Cancer 2009;**9**:57.

38. Zhang Y, Schulte W, Pink D, Phipps K, Zijlstra A, Lewis JD, et al. Sensitivity of cancer cells to truncated diphtheria toxin. PLoS One 2010;**5**:e10498.

39. Kim JS, Jun SY, Kim YS. Critical issues in the development of immunotoxins for anticancer therapy. J Pharm Sci 2020;**109**:104–15.

40. Hessler JL, Kreitman RJ. An early step in pseudomonas exotoxin action is removal of the terminal lysine residue, which allows binding to the KDEL receptor. Biochemistry 1997;**36**:14577–82.

41. Ladokhin AS. pH-triggered conformational switching along the membrane insertion pathway of the diphtheria toxin T-domain. Toxins (Basel) 2013;**5**:1362–80.

42. Lin Y, Wang P, Liu YH, Shang XL, Chen LY, Xue YX. $DT^{270-326}$, a truncated diphtheria toxin, increases blood-tumor barrier permeability by upregulating the expression of caveolin-1. CNS Neurosci Ther 2016;**22**:477–87.

43. Boeva V, Louis-Brennetot C, Peltier A, Durand S, Pierre-Eugène C, Raynal V, et al. Heterogeneity of neuroblastoma cell identity defined by transcriptional circuitries. Nat Genet 2017;**49**:1408–13.

44. van Groningen T, Koster J, Valentijn LJ, Zwijnenburg DA, Akogul N, Hasselt NE, et al. Neuroblastoma is composed of two super-enhancer-associated differentiation states. Nat Genet 2017;**49**:1261–6.

45. Kanato Y, Kitajima K, Sato C. Direct binding of polysialic acid to a brain-derived neurotrophic factor depends on the degree of polymerization. Glycobiology 2008;**18**:1044–53.

46. Sato C, Kitajima K. Polysialylation and disease. Mol Aspects Med 2021;**79**:100892.

47. Cress BF, Englaender JA, He W, Kasper D, Linhardt RJ, Koffas MAG. Masquerading microbial pathogens: Capsular polysaccharides mimic host-tissue molecules. FEMS Microbiol Rev 2014;**38**:660–97.

48. Bartish M, Del Rincón SV, Rudd CE, Saragovi HU. Aiming for the sweet spot: Glyco-immune checkpoints and γδ T cells in targeted immunotherapy. Front Immunol 2020;**11**:564499.

49. Ribeiro AJM, Holliday GL, Furnham N, Tyzack JD, Ferris K, Thornton JM. Mechanism and catalytic site atlas (M-CSA): A database of enzyme reaction mechanisms and active sites. Nucleic Acids Res 2018;**46**:D618–23.

Figure legends

Figure 1. Endosialidase fusion protein selectively internalizes into polysialic acid-expressing cells. **A,** Internalization of GFP-endoNA2 (green) into polysialic acid-containing human neuroblastoma kSK-N-SH cells over a 24-h incubation period at 37°C. Internalization was monitored simultaneously by staining of surface-expressed polysialic acid (red). Note that the kSK-N-SH cell line shows at least two distinct cell populations, the rounded neuritic N-type cells (N) rich in polysialic acid and the flat S-type cells (S) containing low or undetectable amounts of polysialic acid. **B,** Incubation of kSK-N-SH cells with GFP-endoNA containing catalytically active endosialidase (green) for 1 or 24 h at 37°C. **C,** Inhibition of GFP-endoNA2 (green) internalization into kSK-N-SH cells after 1 h of incubation at 37°C by incubation in the presence of excess free polysialic acid or removal of cell surface polysialic acid with endosialidase pretreatment. **D,** Polysialic acid-negative human neuroblastoma SK-N-AS cells were incubated with GFP-endoNA2 (green) for 30 min or 24 h at 37°C. Control cells fixed with paraformaldehyde were stained for surface-expressed polysialic acid (green). **E,** The impact of low temperature or metabolic energy depletion on GFP-endoNA2 (green) internalization. kSK-N-SH cells were either preincubated for 30 min at 4°C or with NaN_3 and 2-DG (2-deoxy-D-glucose) or CCCP at 37°C, followed by incubation for 1 h with GFP-endoNA2. As a control for CCCP-induced mitochondrial depolarization, mitochondria were labeled by pulsing with MitoTracker Red (red) for 15 min at 37°C before depolarization with CCCP. Nuclei were stained with DAPI (blue). Representative images from two to three biological replicates are shown. Scale bars, 20 µm.

Figure 2. Endocytosis of endosialidase fusion protein involves endosomal acidification. **A,** GFP-endoNA2 is colocalized with early endosomes. kSK-N-SH cells were incubated with GFP-endoNA2 (green) for 30 min at 37°C and the fixed cells were immunostained for the early-endosomal marker EEA1 (red). Arrows indicate examples of endosomes containing both GFP-endoNA2 and EEA1. Scale bar, 10 µm. **B,** Internalization in the presence of endosome acidification inhibitors. kSK-N-SH cells were preincubated for 15 min at 37°C with the drug indicated, followed by a further incubation of 1 h with GFP-endoNA2. To monitor for the pH change of acidic intracellular vesicles, cells were stained with acridine orange (AO) for 15 min at 37°C. Nuclei were stained with DAPI (blue). Representative images from two to three biological replicates are shown. Scale bars, 20 µm.

Figure 3. Endosialidase–diphtheria toxin conjugates are highly toxic to neuroblastoma cells. **A,** Schemes of endosialidase fusion constructs used in this study. All proteins have an N-terminal histidine tag. The natural mutations (H417Y and N489D) located on the active site of the non-catalytic endosialidase are indicated by asterisks whereas arrows or arrowheads, respectively, indicate amino acid insertions or substitutions.

Numbers in parentheses indicate the total number of amino acids in each construct. **B** and **C,** Cytotoxic effect of diphtheria toxin (**B**) or *Pseudomonas* exotoxin A (**C**) fusion proteins on kSK-N-SH neuroblastoma cells, determined by cell viability assay. Cells were incubated with increasing concentrations of toxin conjugates or control protein and viability determined at 24 h. The data represent mean ± SD of three to four independent experiments. **D,** The effect of incubation time on cytotoxicity of DT386F-endoNA2. Cells were treated with the conjugate for 2–6 h (pulse period), then cultured in conjugate-free media to 24 h (chase period) and subjected to cell viability assay. Alternatively, cells were incubated with the conjugate continuously for 24 or 48 h. IC_{50} results are expressed as mean ± SD of three to four independent experiments. **E** and **F**, Quantification of DT386F-endoNA2–induced cell apoptosis. kSK-N-SH cells were treated with DT386F-endoNA2 or control V5-endoNA2 for 24 h, and then, cells were stained with annexin V and propidium iodide (PI) (**E**), or CellEvent Caspase-3/7 Green Detection Reagent (**F**). At least 300 cells were quantified for each condition. Results are expressed as mean ± SD of three (**E**) or two (**F**) independent experiments with *, $P < 0.05$; **, $P < 0.01$ and ***, $P < 0.001$ by the Student *t* test.

Figure 4. Selective elimination of polysialic acid-expressing cells after specific binding and internalization of DT386F-endoNA2. **A,** Cytotoxicity of V5-tagged DT386F-endoNA2 on kSK-N-SH cells. Cells were treated with the V5-tagged or untagged conjugate or control protein for 24 h. The data represent the mean ± SD of three independent experiments. **B,** Binding of V5-DT386F-endoNA2 to kSK-N-SH cells. 100 nM conjugate or control protein was added onto the fixed cells, incubated for 1 h at room temperature and immunostained for V5 (red). **C,** Internalization of V5-DT386F-endoNA2 into kSK-N-SH cells. The cells were incubated with 100 nM conjugate or control protein for 2 or 24 h at 37°C or 2h at 4°C, fixed, and immunostained for V5 (red). As a control, free polysialic acid was used to strip off the bound conjugates from the cell surface by competition. Examples of N-type (N) and S-type (S) cells are indicated. **D,** Effect of prolonged exposure of kSK-N-SH cells to DT386F-endoNA2. The cells were incubated with 10 nM conjugate for 72 h at 37°C. After incubation, the cells were fixed and stained for surface-expressed polysialic acid (green). The proportion of flat S-type cells is indicated below the images and the values represent the means of three randomly chosen fields ± SD of a single experiment. For each field, at least 100 cells were examined. Cells incubated without conjugate or with DsRed-endoNA2 were used as controls. Nuclei were stained with DAPI (blue). Representative images from two to three biological replicates are shown. Scale bars, 20 μm.

Figure 5. Cytotoxicity of DT386F-endoNA2 against malignant neuroblastoma cells and non-malignant primary cells. **A** and **B,** The cytotoxic activity of DT386F-endoNA2 was tested against neuroblastoma SK-N-SH and SH-SY5Y cells expressing low or intermediate levels of polysialic acid (polySia+), respectively, and polysialic acid-negative (polySia−) SK-N-AS cells (**A**) as well as fibroblast BJ cells and normal bone marrow

mononuclear cells from two healthy donors (donor 1 and 2) (**B**). Cells were treated with the conjugate or control protein for 24 h and viability was measured using cell viability assay. The data represent the mean ± SD of three independent experiments.

Figure 6. Characteristics of the intrinsic cytotoxicity of truncated diphtheria toxin domain on malignant cells. **A,** Cytotoxicity of DT386 alone or DT386 fused via a furin-cleavable linker with catalytically active endosialidase compared with DT386F-endoNA2. kSK-N-SH cells with high expression of polysialic acid were treated with the conjugate indicated for 24 h and subjected to cell viability assay. **B,** The effect of incubation time on cytotoxicity of DT386 or DT386F-endoNA. Cells were treated with the conjugate indicated for 2–6 h (pulse period), cultured in conjugate-free media to 24 h (chase period) and subjected to cell viability assay. Data from Fig. 3D is shown for comparison. **C** and **D,** Comparison of cytotoxic activity of DT386 and DT386F-endoNA2 on malignant (**C**) and non-malignant cells (**D**). Polysialic acid-containing (polySia+) neuroblastoma SH-SY5Y cells and polysialic acid-negative (polySia−) neuroblastoma SK-N-AS cells, fibroblast BJ cells and normal bone marrow mononuclear cells from healthy donor (donor 2) were treated and analyzed as in (**A**). The data represent the mean ± SD of three independent experiments.

Figure 1

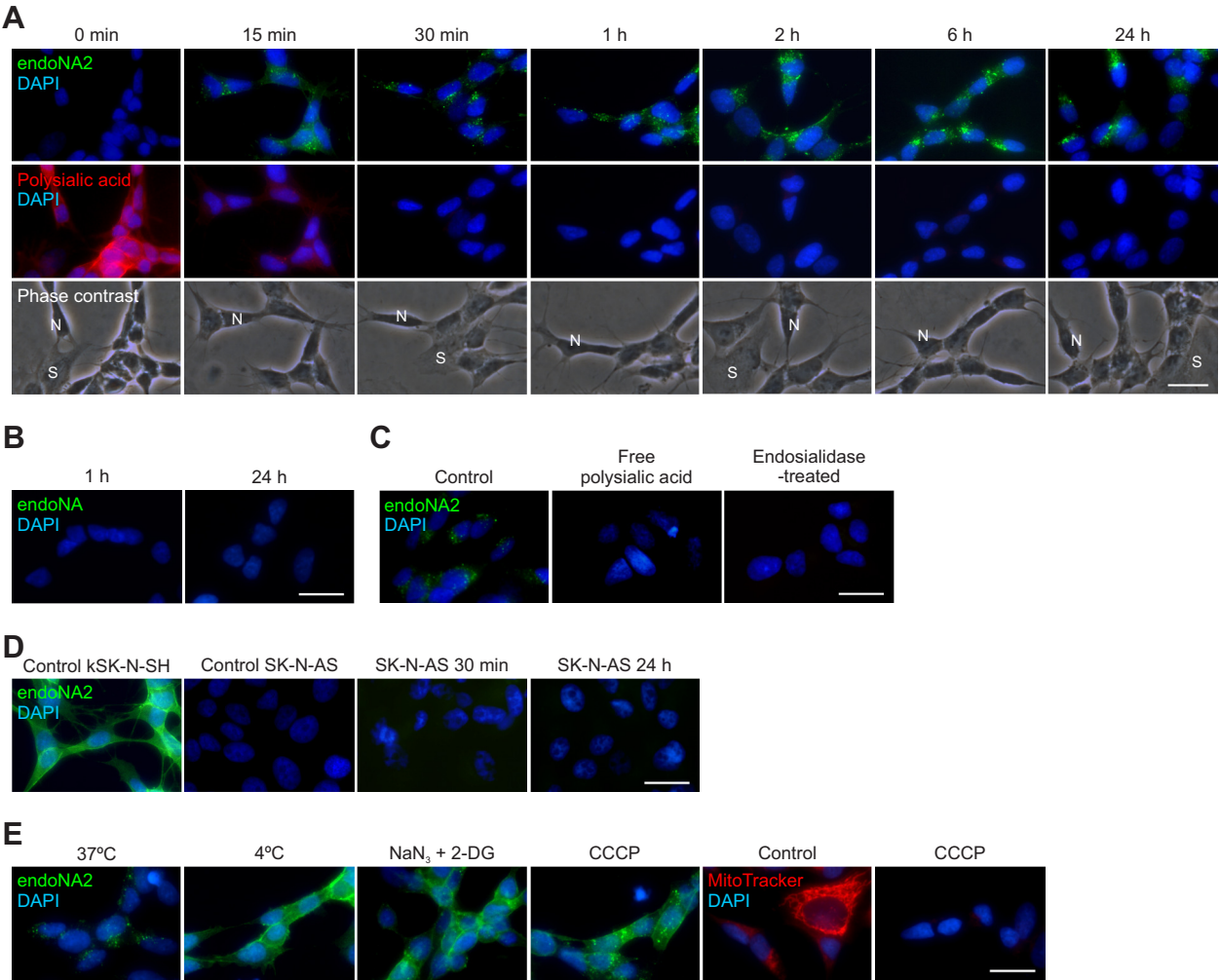
A
0 min
15 min
30 min
1 h
2 h
6 h
24 h
endoNA2
DAPI
Polysialic acid
DAPI
Phase contrast
N
S
B
1 h
24 h
endoNA
DAPI
C
Control
Free
polysialic acid
Endosialidase
-treated
endoNA2
DAPI
D
Control kSK-N-SH
Control SK-N-AS
SK-N-AS 30 min
SK-N-AS 24 h
endoNA2
DAPI
E
37ºC
4ºC
NaN3 + 2-DG
CCCP
Control
CCCP
endoNA2
DAPI
MitoTracker
DAPI

Figure 2

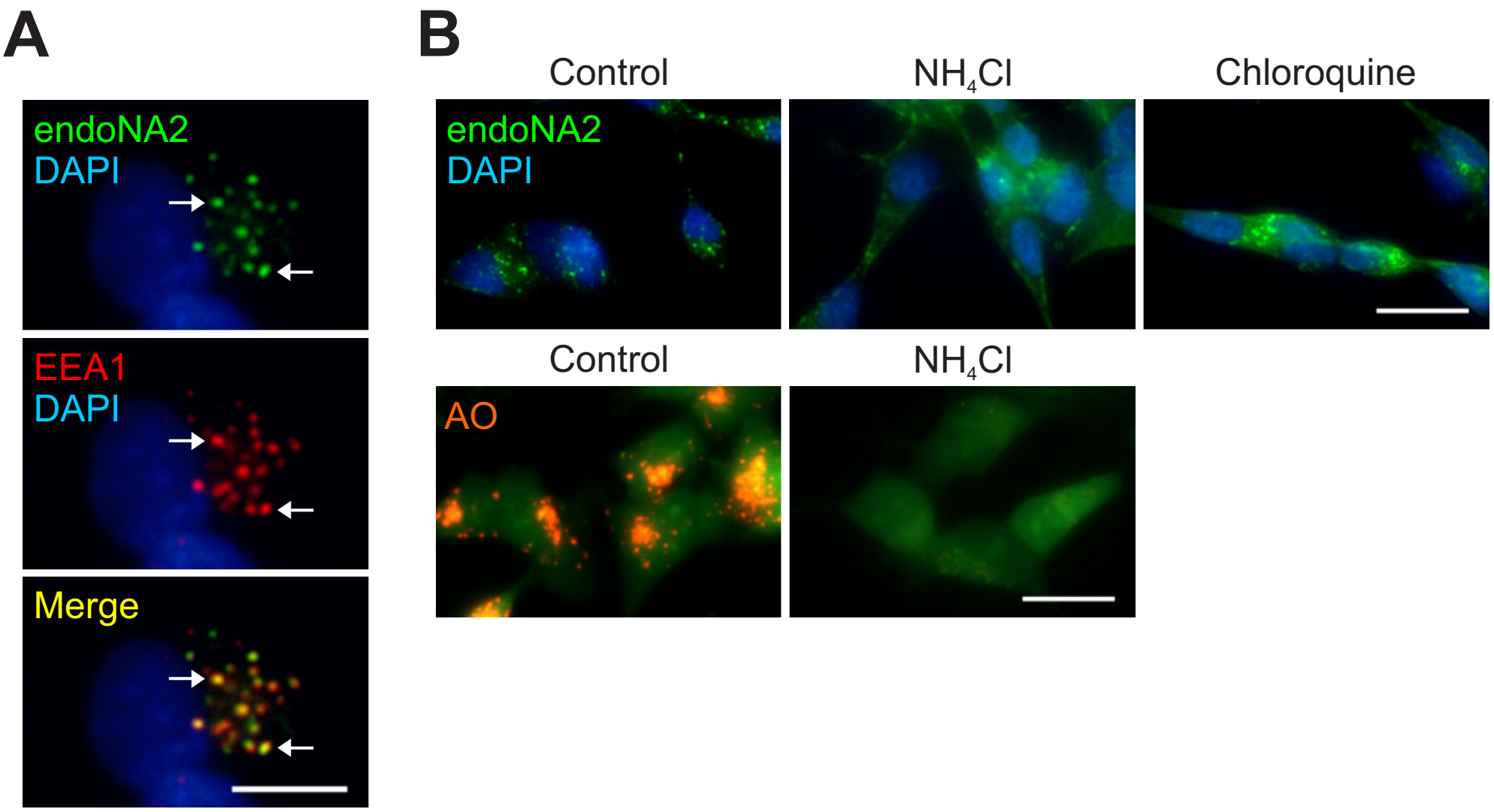
A
endoNA2
DAPI
EEA1
DAPI
Merge
B
Control
NH4Cl
Chloroquine
endoNA2
DAPI
Control
NH4Cl
AO

Figure 3

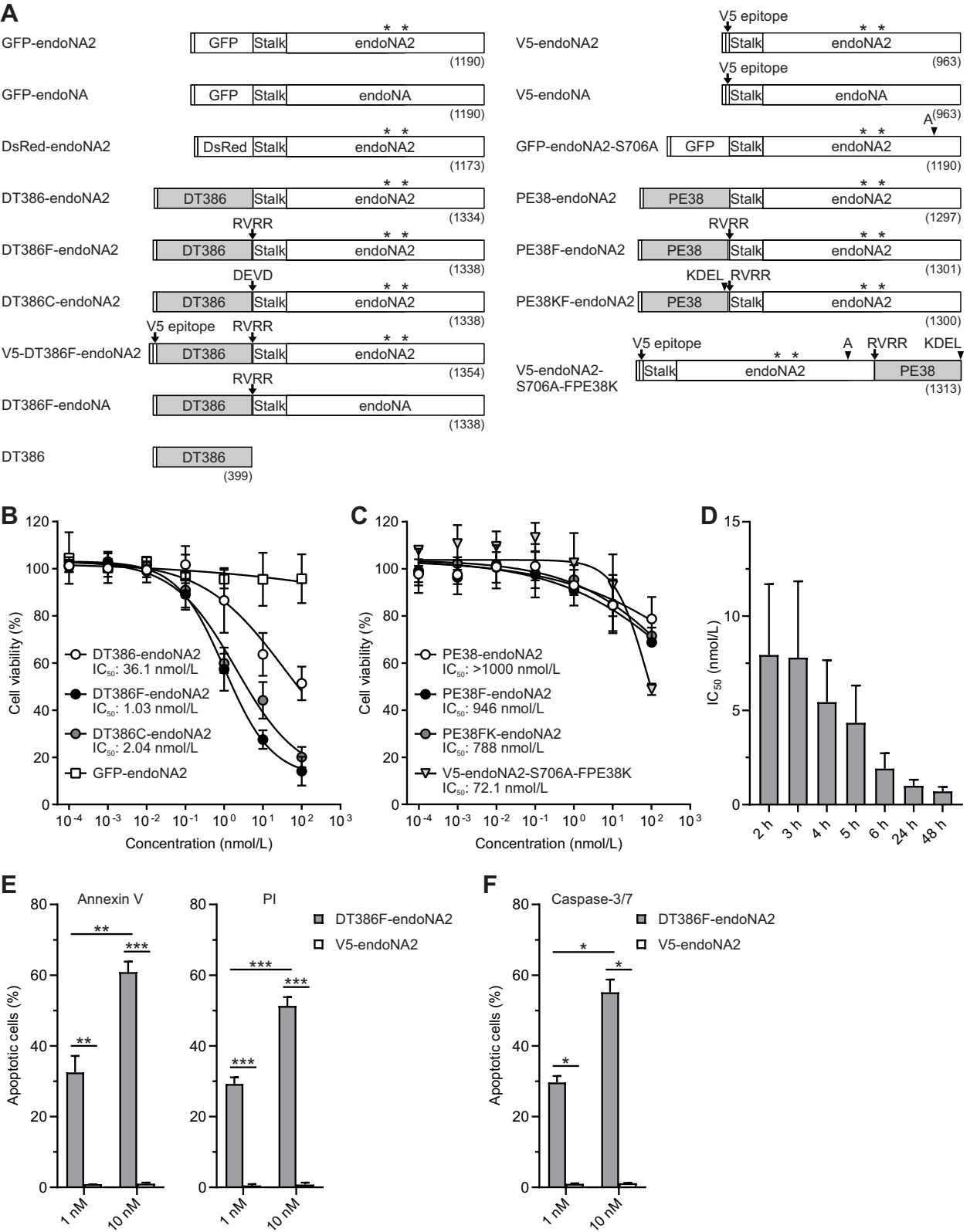
A
GFP-endoNA2
GFP
Stalk
endoNA2
(1190)
GFP-endoNA
endoNA
(1190)
DsRed-endoNA2
DsRed
(1173)
DT386-endoNA2
DT386
(1334)
RVRR
DT386F-endoNA2
(1338)
DEVD
DT386C-endoNA2
V5 epitope
V5-DT386F-endoNA2
(1354)
DT386F-endoNA
(1338)
DT386
(399)
V5-endoNA2
(963)
V5-endoNA
A(963)
GFP-endoNA2-S706A
(1190)
PE38-endoNA2
PE38
(1297)
PE38F-endoNA2
(1301)
KDEL
PE38KF-endoNA2
(1300)
A
V5-endoNA2-
S706A-FPE38K
(1313)
B
Cell viability (%)
DT386-endoNA2
IC50: 36.1 nmol/L
DT386F-endoNA2
IC50: 1.03 nmol/L
DT386C-endoNA2
IC50: 2.04 nmol/L
GFP-endoNA2
Concentration (nmol/L)
C
PE38-endoNA2
IC50: >1000 nmol/L
PE38F-endoNA2
IC50: 946 nmol/L
PE38FK-endoNA2
IC50: 788 nmol/L
V5-endoNA2-S706A-FPE38K
IC50: 72.1 nmol/L
D
IC50 (nmol/L)
2 h
3 h
4 h
5 h
6 h
24 h
48 h
E
Annexin V
PI
DT386F-endoNA2
V5-endoNA2
Apoptotic cells (%)
1 nM
10 nM
F
Caspase-3/7

Figure 4

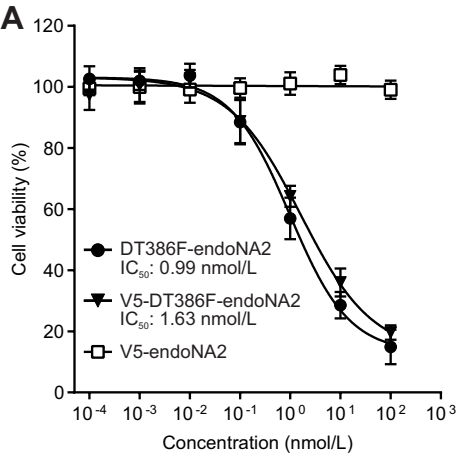
A
120
100
80
60
40
20
0
Cell viability (%)
DT386F-endoNA2
IC50: 0.99 nmol/L
V5-DT386F-endoNA2
IC50: 1.63 nmol/L
V5-endoNA2
10-4 10-3 10-2 10-1 100 101 102 103
Concentration (nmol/L)

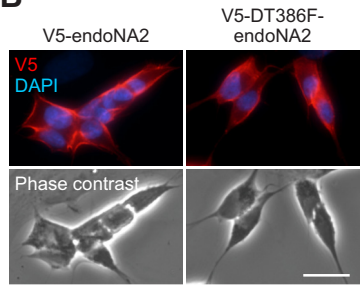
B
V5-endoNA2
V5-DT386F-endoNA2
V5
DAPI
Phase contrast

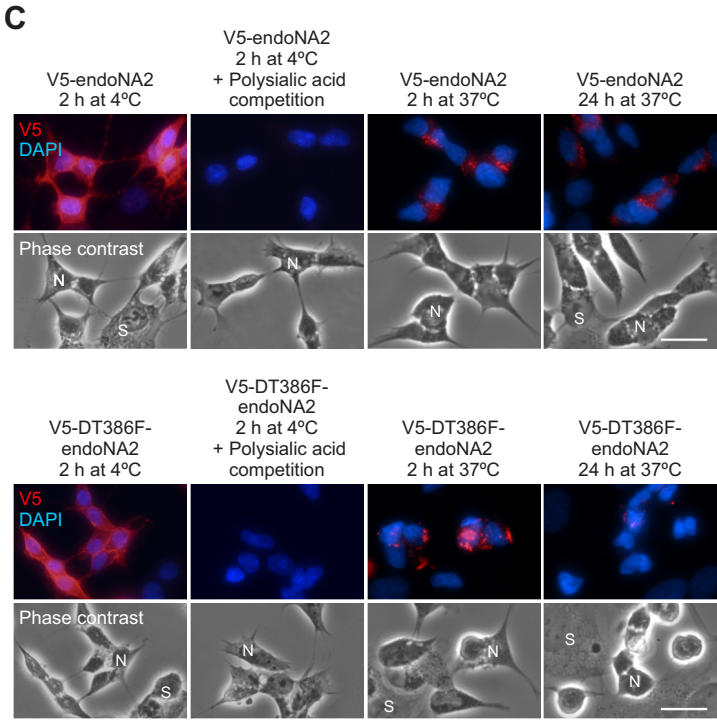
C
V5-endoNA2 2 h at 4ºC
V5-endoNA2 2 h at 4ºC + Polysialic acid competition
V5-endoNA2 2 h at 37ºC
V5-endoNA2 24 h at 37ºC
V5
DAPI
Phase contrast
N
S
V5-DT386F-endoNA2 2 h at 4ºC
V5-DT386F-endoNA2 2 h at 4ºC + Polysialic acid competition
V5-DT386F-endoNA2 2 h at 37ºC
V5-DT386F-endoNA2 24 h at 37ºC

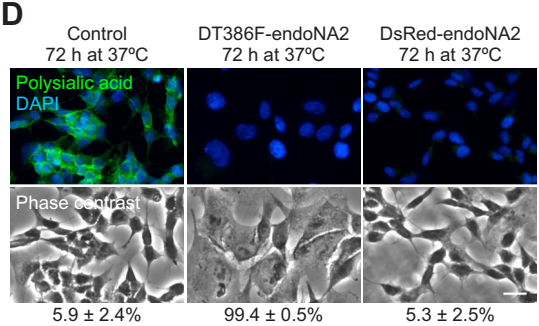
D
Control 72 h at 37ºC
DT386F-endoNA2 72 h at 37ºC
DsRed-endoNA2 72 h at 37ºC
Polysialic acid
DAPI
Phase contrast
5.9 ± 2.4%
99.4 ± 0.5%
5.3 ± 2.5%

Figure 5

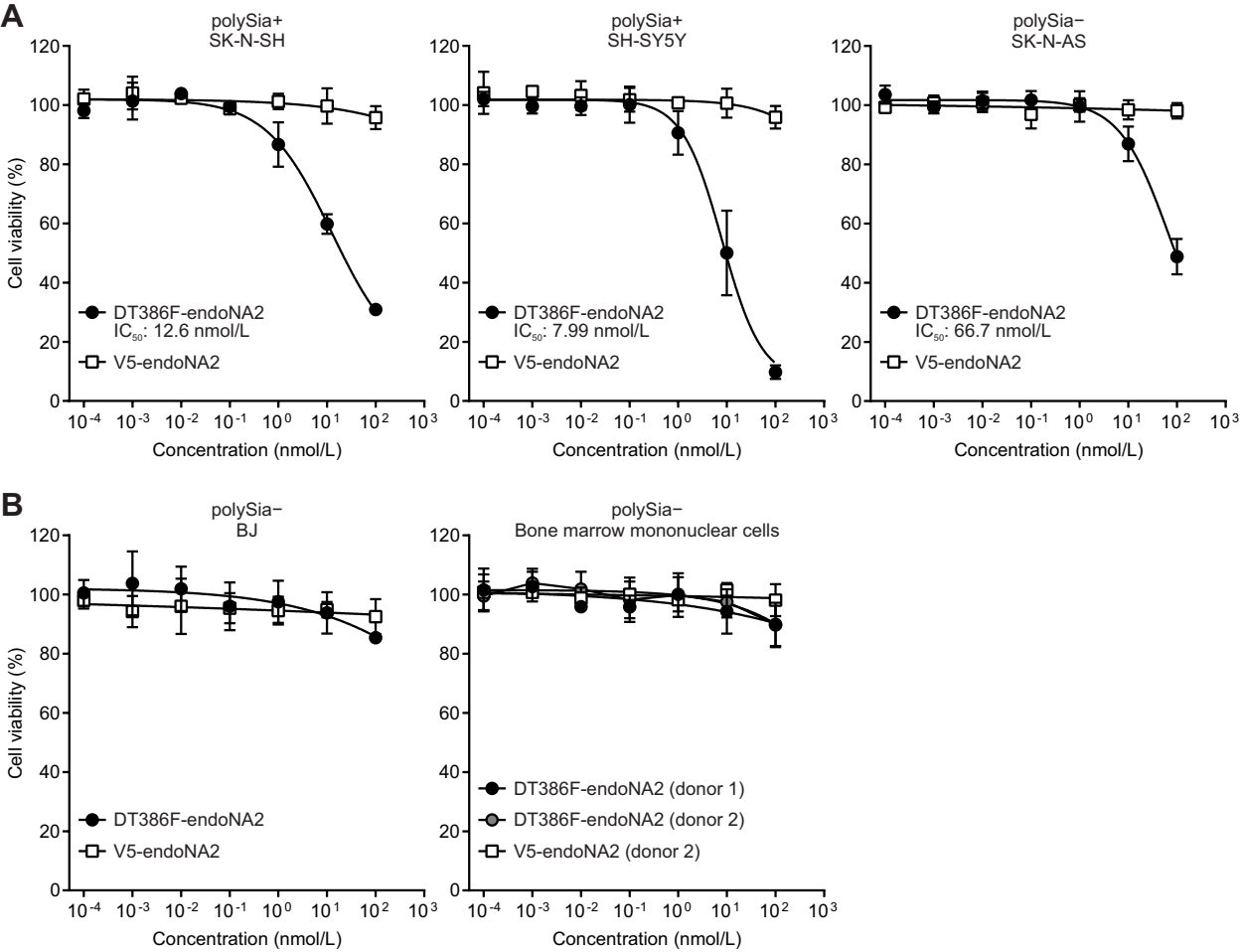
A
polySia+
SK-N-SH
polySia+
SH-SY5Y
polySia−
SK-N-AS
Cell viability (%)
DT386F-endoNA2
IC50: 12.6 nmol/L
V5-endoNA2
DT386F-endoNA2
IC50: 7.99 nmol/L
V5-endoNA2
DT386F-endoNA2
IC50: 66.7 nmol/L
V5-endoNA2
Concentration (nmol/L)
B
polySia−
BJ
polySia−
Bone marrow mononuclear cells
DT386F-endoNA2
V5-endoNA2
DT386F-endoNA2 (donor 1)
DT386F-endoNA2 (donor 2)
V5-endoNA2 (donor 2)

Figure 6

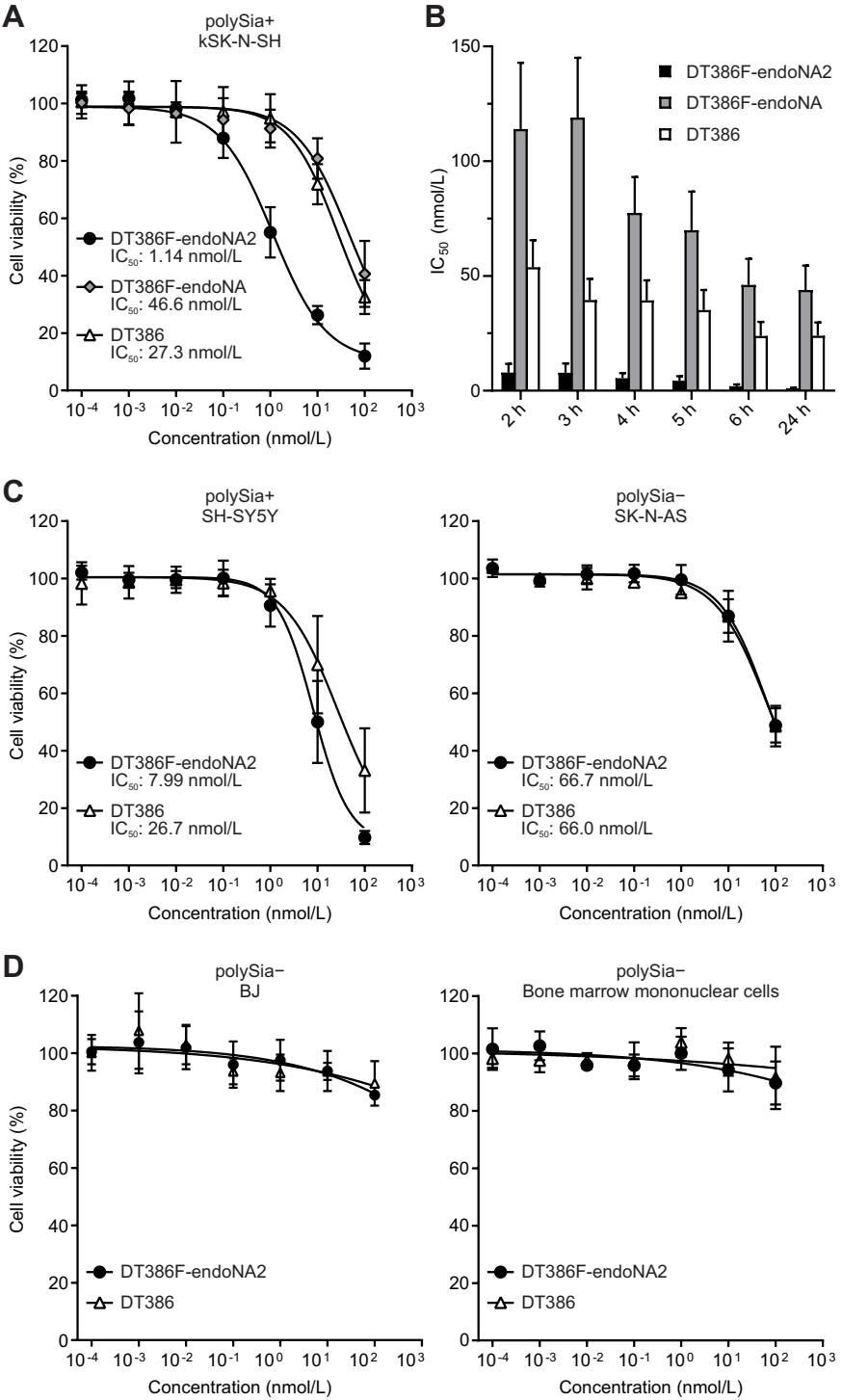
A
polySia+
kSK-N-SH
Cell viability (%)
DT386F-endoNA2
IC50: 1.14 nmol/L
DT386F-endoNA
IC50: 46.6 nmol/L
DT386
IC50: 27.3 nmol/L
Concentration (nmol/L)
B
IC50 (nmol/L)
DT386F-endoNA2
DT386F-endoNA
DT386
2 h
3 h
4 h
5 h
6 h
24 h
C
polySia+
SH-SY5Y
DT386F-endoNA2
IC50: 7.99 nmol/L
DT386
IC50: 26.7 nmol/L
polySia−
SK-N-AS
DT386F-endoNA2
IC50: 66.7 nmol/L
DT386
IC50: 66.0 nmol/L
D
polySia−
BJ
polySia−
Bone marrow mononuclear cells